Journal of Colloid and Interface Science 679 (2025) 403–410

Contents lists available at ScienceDirect

Journal of Colloid And Interface Science

journal homepage: www.elsevier.com/locate/jcis

Discontinuity-enhanced icephobic surfaces for low ice adhesion

Pablo F. Ibáñez Ibáñez [a,b,*], Luca Stendardo [b], Catalina Ospina [b], Rajat Chaudhary [b,c], Irene Tagliaro [b], Carlo Antonini [b,*]

[a] Laboratory of Surface and Interface Physics, Department of Applied Physics, University of Granada, Granada 18071, Spain
[b] Laboratory of Surface Engineering and Fluid Interfaces, Department of Materials Science, University of Milano-Bicocca, Milano 20125, Italy
[c] Glass & Ceramics Lab, Department of Industrial Engineering, University of Trento, Trento 38123, Italy

GRAPHICAL ABSTRACT

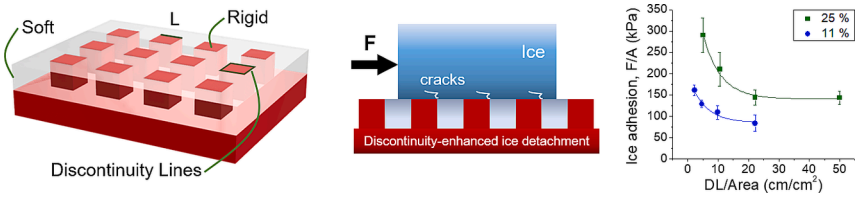

ARTICLE INFO

Keywords:
Icephobic
Interfacial fracture
Durable surfaces
Low ice adhesion

ABSTRACT

Hypothesis: Passive low ice-adhesion surfaces are frequently composed of soft materials; however, soft materials potentially present durability issues, which could be overcome by fabricating composite surfaces with patterned rigid and soft areas. Here we propose the innovative concept of discontinuity-enhanced icephobic surfaces, where the stress concentration at the edge between rigid and soft areas, i.e. where discontinuities in elasticity are located, facilitates ice detachment.

Experiments: Composite model surfaces were fabricated with controlled rigid-soft ratios and discontinuity line lengths. The ice adhesion values were measured while recording the ice/substrate interface, to unravel the underpinning ice detachment mechanism. The experiments were complemented by numerical simulations that provided a better understanding of the ice detachment mechanism.

Findings: It was found that when a surface contains rigid and soft areas, stress is concentrated at the edge between soft and hard areas, i.e. at the discontinuity line, rather than all over the soft or rigid areas. An unexpected non-unidirectional crack propagation was observed for the first time and elucidated. When rigid and deformable materials are present, the crack occurs on the discontinuity line and propagates first on rigid and then on soft areas. Moreover, it was demonstrated that an increase in discontinuities promotes crack initiation and leads to a reduction of ice adhesion.

1. Introduction

Icing is a natural phenomenon affecting daily life and safe operations in diverse areas, spanning from aeronautics to ground transportation, communication and power systems (such as power lines, wind turbines or solar panels). From the dramatic accident in 2009 of the Air France Flight 447 flying from Rio de Janeiro to Paris, where ice crystals obstructed the aircraft pitot tubes, causing the death of all 228

* Corresponding authors.
E-mail addresses: pabloi@ugr.es (P.F. Ibáñez Ibáñez), carlo.antonini@unimib.it (C. Antonini).

https://doi.org/10.1016/j.jcis.2024.09.205
Received 2 July 2024; Received in revised form 19 September 2024; Accepted 26 September 2024
Available online 26 September 2024

passengers and crew, to close-to-ground operation of drones for last-mile delivery, energy-efficient and environmentally sustainable ice protection solutions are needed for human safety. Within this framework, the interest in surfaces with icephobic properties has flourished in the last decade due to their potential application for increased safety and reduced energy consumption in icing conditions [1–5]. The Holy Grail for ideal icephobicity would be a one-fits-all durable surface, combining all the desirable properties of ice nucleation delay and freezing point reduction [6–11], or, in case freezing happens, ice accretion reduction [6,7] and low ice adhesion, to facilitate deicing [12–15]. It is also desirable for icephobic surfaces to be PFAS-free, due to rising concerns on the potential toxicity of some perfluoroalkyl substances [16,17]. Although such ideal surfaces have yet to be developed, low elastic modulus materials have been proven to be a possible solution for easier ice release, as they present low ice adhesion strength due to their ability to deform, creating stress concentrations at the ice-substrate interface [14,18] that facilitate ice detachment.

Recently, conceptually new types of surfaces are emerging as promising solutions. An example are the low interfacial toughness materials, that propose easy ice detachment at constant force when the iced area is large; such materials take advantage of the toughness-dominated ice detachment mechanism, which is different from the stress-dominated regime, where the ice detachment force scales with the ice-substrate interface area [19]. Other surfaces take advantage of a specific material property discontinuity, such as thermal conductivity, to reduce intrinsic ice adhesion due to interfacial expansion stress during the freezing process [20].

Discontinuities at the nano and micro-scale play an important role in controlling interfacial phenomena: as an example, surface wetting discontinuities have been studied to improve heat transfer efficiency in phase-change phenomena, such as water condensation and boiling [21,22]. Concerning icing, studies have suggested that hollow structures in pure material [23–25] or the combination of materials with different elastic moduli [26–28] can facilitate ice shedding. Such studies are based on the assumption that stress concentrations can promote crack initiation and propagation, starting mostly on the softer part. However, direct experimental proof of this assumption is not straightforward, even if it was shown with microscope imaging [26] and properly analyzed [23]. Surface elasticity can also be combined with other properties, such as low interfacial toughness or a quasi-liquid lubricating layer with hollow structures [1,29,30], to further reduce ice adhesion. Nevertheless, mechanical durability represents a major bottleneck for such surfaces, which in many cases are based on soft polymers, and therefore durability and icephobicity must reach a compromise [31–35].

In this study, we present the new concept of discontinuity-enhanced icephobic surfaces, leading to low ice adhesion. To demonstrate the concept, we fabricated a composite rigid-soft model surface, consisting of a patterned interface alternating rigid areas made of epoxy resin with soft areas of PDMS (polydimethylsiloxane), to produce a rigid-soft interface with sharp discontinuities in mechanical properties. Ice adhesion tests demonstrate that on such discontinuity-enhanced icephobic surfaces ice adhesion can be reduced by an order of magnitude, compared to standard materials such as aluminum, glass, or hard polymers. Specifically, increasing the discontinuity density promotes crack initiation and leads to ice adhesion reduction, while preserving excellent abrasion resistance due to the mechanical properties of hard regions. In addition, we provide direct observation of crack initiation at the discontinuities, unravelling an unexpected non-unidirectional crack propagation, initiated at the discontinuity and propagating first on the rigid and later in the soft areas: as such, we address the challenge to the classical framework of ice adhesion failure mechanism and explain the underpinning ice detachment mechanism with the support of experimental and numerical approaches.

2. Materials and methods

2.1. Samples preparation

Surfaces with a heterogeneous elasticity distribution were prepared by filling a polymeric 3D printed rigid structure with a soft material. The spatial resolution of the printing technique was 50 μm and the layer thickness was also set to 50 μm, see supplementary material for further details. The rigid structures consisted of substrates with patterns of uniformly distributed square pillars, see Fig. 1A. The patterns were prepared with two spacings: distance between pillars of the same width as the pillars and, distance between pillars two times the width of the pillars. Consequently, the ratio of surface covered with pillars is 25 % and 11.1 % respectively. This ratio is equivalent to the ratio of rigid area after the filling with the soft polymer. In addition, samples were prepared with 4 different widths for the pillars: 200, 450, 950, and 2000 μm (see Fig. 1B), covering an order of magnitude and maintaining a uniform distribution in logarithmic scale. The selected sizes allow us to visualize the crack generation and propagation on the rigid areas. These four different pillar widths allow the variation of the Discontinuity Line (DL) length, that is the sum of all the rigid-soft edges, i.e. the perimeter of the pillars. Analogously, the discontinuity line density is the length of the rigid-soft border per unit of area (thus it is expressed dimensionally as cm/cm^2). The spaces between the rigid pillars were filled using a syringe with liquid polydimethylsiloxane (PDMS Sylgard 184 mixed in 1:10 ratio). Then the samples were cured at 80 °C for 120 min to crosslink the soft polymer. The level reached by the soft polymer is very similar to the height of the rigid pillars, obtaining a visually uniform rigid-soft surface. The soft part never overflows the pillars, see Figures S2 and S3. In addition, samples with homogeneous elasticity of the rigid and soft materials were prepared for comparison. To evaluate the durability of the surfaces, some of the replicas were manually abraded using P600 sandpaper under a pressure of 200 kPa.

2.2. Ice adhesion measurements

The ice adhesion values to the different surfaces were evaluated employing a home-made horizontal shear test described elsewhere [36,37], see Figure S1. In this setup, a hollow cylinder of 12 mm internal diameter is placed over the sample and filled with distilled water up to 5 mm height. Then, the sample is cooled down to −10 °C using a Peltier plate situated below the sample while the relative humidity is maintained under 2 %. After total freezing, the tip of a commercial force sensor (*Mark-10, Force Gauge M5-20*) pushes the cylinder at a height of 3 mm from the surface and with a velocity of 0.01 mm/s until total detachment. A picture of the setup can be found in the supplementary material, subsection “Ice adhesion measurements”. The shear ice adhesion strength is calculated as F/A, where F is the peak force and A is the interfacial area. A total of 8 measurements were performed with the ice block randomly placed over the samples.

2.3. Interfacial fracture recording

The ice detachment process was recorded from top view for the qualitative analysis of the interfacial fracture mechanism. Clear visualization of the interface is possible because the slow freezing process, 20 min, allows to obtain transparent ice (further explanation in supplementary material). The recording was performed for all the measurements using a phone camera at 60 fps with a resolution of 1920 × 1080 pixels using a 4 × digital zoom. Moreover, some recordings were performed in detail using a high-speed camera (*Photron, Fastcam Nova S6*) at 1000 or 2000 fps with a resolution of 1024 × 1024 pixels.

2.4. Samples characterization

In addition, different properties of the employed materials were

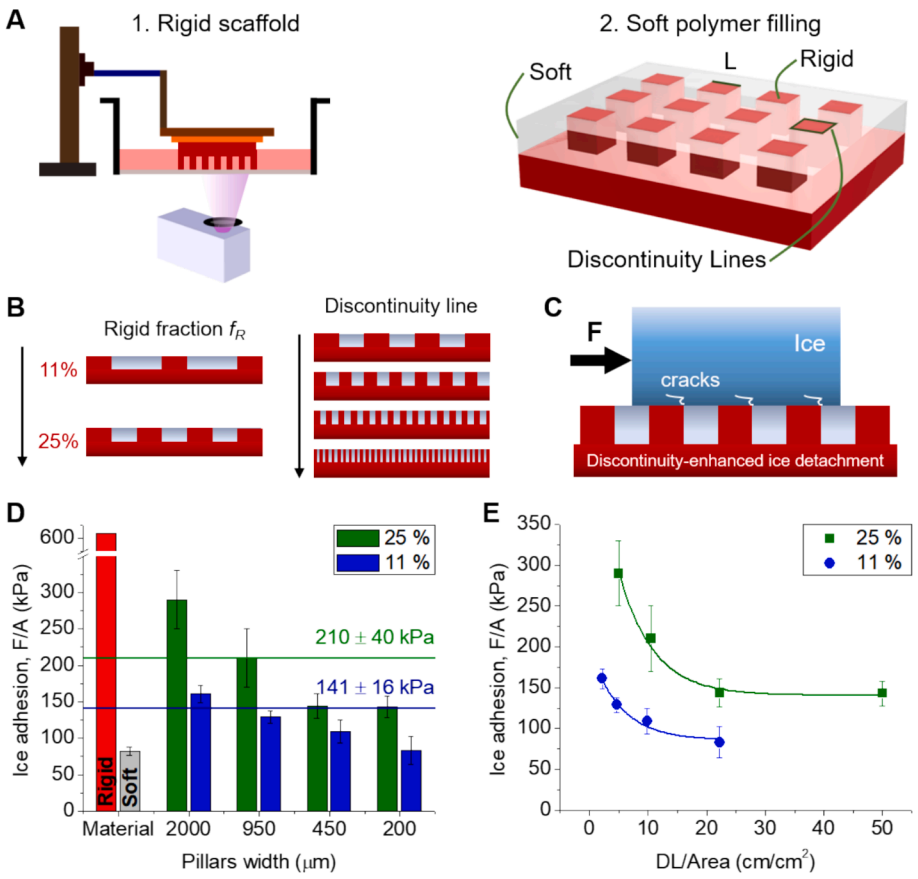

Fig. 1. Discontinuity-enhanced icephobicity concept and ice adhesion strength results. A) Schematic process of the two-step surface fabrication: (i) 3D printed rigid scaffold consisting of pillar-textured photopolymerized resin (E = 1150 MPa), using digital light processing, and (ii) soft polymer filling with PDMS (E = 1.7 MPa). The resulting surface is smooth, with discontinuous mechanical properties. B) Representation of surfaces with different rigid fractions, f_R (11 % and 25 %) by changing the pillar distance, and different discontinuity line density, by controlling the pillar width, L (200–2000 μm) for a given f_r. C) Schematic representation of the push test, showing that cracks are initiated on discontinuities. D) Comparison of ice adhesion strength with different rigid pillars width and two fractions of rigid area with pristine rigid and soft materials. The blue and green horizontal lines correspond to the weighted averages $F/A = f_r(F/A)_r + f_s(F/A)_s$, based on the rigid fraction of 11 % and 25 %, respectively. The error bar for rigid material is not represented, its value is 140 kPa. E) Ice adhesion as function of the discontinuity line density (DL/Area). (For interpretation of the references to color in this figure legend, the reader is referred to the web version of this article.)

characterized, such as elastic modulus (E), Advancing and Receding Contact Angles (ACA and RCA), surfaces topography and roughness. For brevity, the description of these methods along with extended versions of sample preparation and ice adhesion measurements can be found in the supplementary material section "Detailed materials and methods".

2.5. Numerical modeling

The ice-substrate interface stresses are computed with a finite-element method (FEM) numerical simulation. The model consists of a complex rigid-soft surface, an ice column, and a nylon mold, which mimic the experimental setup. A similar numerical model has been utilized previously elsewhere [36,37]. The force application on the outside of the mold is simulated by imposing the displacement of an area of 1 × 1 mm^2. This area corresponds to the estimated contact surface between the force application rod and the nylon mold in the experimental case. The materials used in the simulation were modeled as isotropic elastic with the properties presented in Table 1.

The interface stresses are computed by static structural analysis (Ansys Mechanical 2020 R1). Mesh independence is confirmed and presented in Figure S7 and Table S3.

To analyze the interface stresses, an arbitrary, constant displacement value is applied on the dedicated area on the outside of the mold. As all the materials are modeled as perfectly elastic, equal forces are applied on all the analyzed cases. By comparing the interface stresses of different surface geometries, the configuration that leads to the highest stress concentrations is identified.

Table 1
Density, elastic modulus, and Poisson ratio of the materials. The properties of ice are taken from literature [38].

Material	ρ (kg/m^3)	E (MPa)	ν
Resin	1059	1150	0.35
PDMS	965	1.5	0.45
Ice	915	9000	0.31
Nylon	1140	1500	0.39

3. Results and discussion

3.1. Ice adhesion of discontinuity-enhanced surfaces

The underlying assumption of this study is that the introduction of surface elasticity discontinuities can promote ice crack initiation, resulting in discontinuity-enhanced icephobicity. To test this hypothesis and to demonstrate that an increase in discontinuities leads to a decrease in ice adhesion, we developed model surfaces with a controlled pattern with characteristic lengths ranging from 200 μm to 2 mm, large enough to allow optical visualization. A scheme of the model surfaces can be seen in Fig. 1A. Surfaces were designed and prepared in two steps, first

by 3D printing a rigid pillar pattern by digital light processing (DLP) using a photopolymerizable resin, then by filling the interpillar voids with a soft polymer, PDMS (see materials properties in Table S1). Rigid fractions, calculated as rigid area over total area, $f_r = A_r/A_{tot}$ were designed equal to 11 % and 25 % (see measured values in Table S2) using four different pillar lateral widths, L (200 μm to 2 mm) to modify the discontinuity line density, a scheme can be seen in Fig. 1B. We refer to the rigid-soft interface as *Discontinuity Line* (DL), scaling as 1/L, as L is the pattern characteristic length: for a given rigid fraction, the smaller the pillars, the longer the DL between rigid and soft materials. Detailed pictures of the surfaces and pillars are shown in Figure S2. The role of discontinuities can thus be assessed by ice adhesion tests (see Fig. 1C). In case discontinuities play no effect, the ice adhesion force would result in a weighted average between the ice adhesion on the rigid area, $(F/A)_r = 610 \pm 140$ kPa, and the soft area, $(F/A)_s = 82 \pm 6$ kPa, and would be independent of the pillars dimension. In this scenario, it may be possible to express adhesion as a weighted average, e.g. $F/A = f_r(F/A)_r + f_s(F/A)_s$, based on the rigid and soft fractions, f_r and f_s, analogously to wetting of heterogeneous surfaces, for which the Cassie-Baxter equation predicts the cosine of contact angles as: $cos\theta_{CB} = f_1 cos\theta_1 + f_2 cos\theta_2$. In contrast, if discontinuities promote interfacial cracks [23,24,28], ice adhesion force should decrease with longer DL, i.e. on surfaces with smaller pillars.

The results of the ice adhesion tests are shown in Fig. 1D and E. The ice adhesion strength presents a clear trend, with the ice adhesion reducing for decreasing pillar width; a similar trend is observed for both rigid fractions (11 % and 25 %). For the largest pillar width, 2 mm, the adhesion value is higher than the weighted average ($F/A = f_r(F/A)_r + f_s(F/A)_s$). However, the adhesion is lower for the rest of the samples. Most interestingly, the ice adhesion on the sample with $f_r = 11\%$ and the longest DL equals the value of pure soft material (PDMS).

To evaluate the mechanical durability of the proposed surfaces, the ice adhesion value was also measured after harsh abrasion with sandpaper (Fig. 2A). In Figure S3 we can observe the surface change before and after abrasion, Table S1 shows material's properties after abrasion. The abraded soft material (PDMS) had an ice adhesion strength of 107 ± 13 kPa, while the abraded rigid material (resin) had 1470 ± 210 kPa. Ice adhesion strength increased on both materials, soft and rigid, but the effect of abrasion is higher on the rigid resin: this can be explained by the increase in roughness, which may increase mechanical interlocking and thus adhesion especially on the rigid resin, and with less effect on the soft PDMS, as revealed previously [39]. The ice adhesion values for the abraded rigid-soft surfaces are shown in Figure S3. The general trend confirms that of the non-abraded samples, with the ice adhesion values

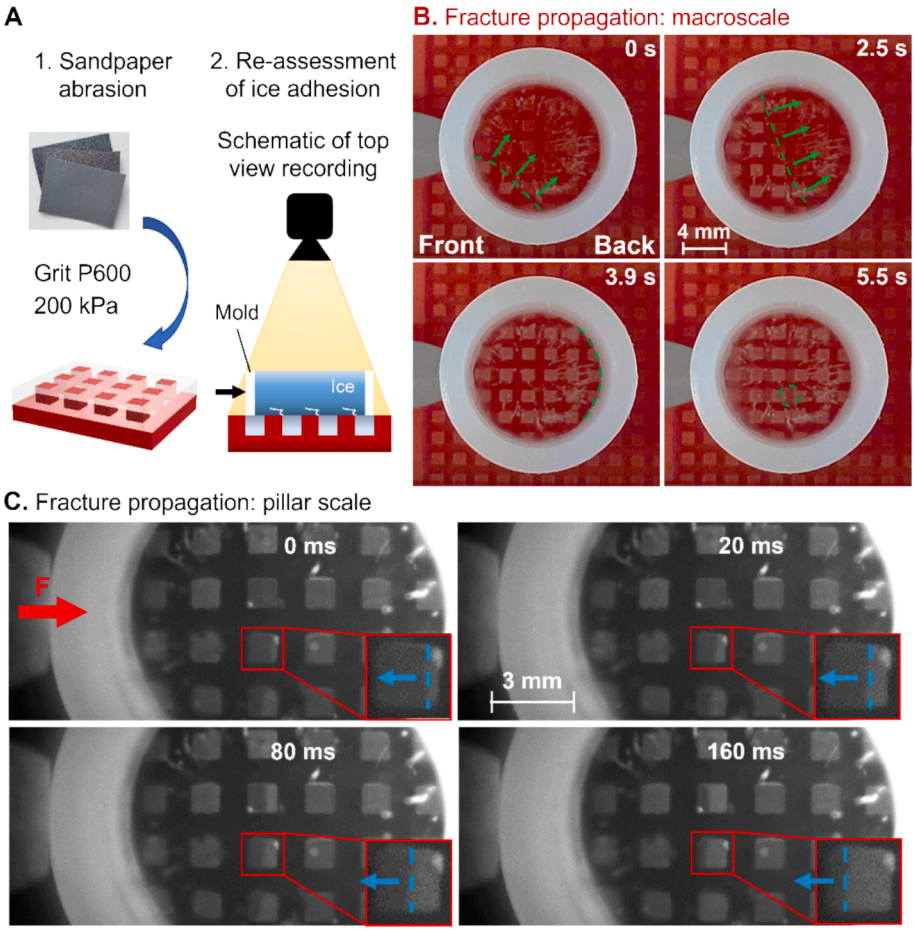

Fig. 2. Mechanism of crack propagation and interface separation for discontinuity-enhanced icephobic surfaces. A) Samples were first abraded and ice adhesion was re-assessed for durability, while recording from the top with both regular camera and high-speed camera to understand the crack propagation on the rigid and soft parts. B) Fracture propagation at the macroscale (full sequence in movie S1): ice detachment begins at the force application point and propagates to the other side of the ice block (for simplicity, referred to as front-to-back propagation, corresponding to left-to-right in the image sequence). The detachment occurs in two stages: first, the ice detaches from the rigid pillars (t ~ 0–5 s, v ~ 2.4 mm/s), then from the soft areas (t ~ 5–8 s). The green lines and arrows indicate the border of the detached area and the propagation direction, the green circle shows a soft area just detached (lighter red color compared to previous frame). C) Fracture propagation at the pillar scale (full sequence in movie S2): on the individual pillar, the crack is initiated on the discontinuity; counterintuitively, the crack starts at the back edge of the pillar, and then propagates (t ~ 0.5 s, v ~ 2 mm/s) over the pillar to the front side, with a crack propagation opposite to the force application. (For interpretation of the references to color in this figure legend, the reader is referred to the web version of this article.)

decreasing as the pillar width decreases. The increase in ice adhesion is indeed due to the greater surface roughness for the investigated model surfaces. However, it is confirmed that the rigid-soft surfaces show a lower ice adhesion than the weighted average of the rigid and soft ice adhesion values. This result confirms the role of discontinuities and demonstrates the abrasion resistance. Therefore, the rigid pillars accomplish their function of increasing surface durability. The adhesion values may depend on the roughness, i.e. the grit number of the sandpaper, and the resistance of the pillar structure may depend on the hardness of the material employed, which can be further optimized to improve mechanical resistance.

3.2. Fracture mechanism analysis

To understand the working principle of these surfaces, it is essential to analyze the detachment process. For this reason, the ice-substrate interface was recorded during ice detachment with a standard and with a high-speed camera (see materials and methods for details). For the non-abraded samples, the detachment process is about one order of magnitude faster, so it is only observable under high-speed camera recording. The detachment process is slower on the abraded surfaces because cracks do not propagate in a steady and continuous manner, since the asperities on the interface act as barriers, where the crack tip stalls and micro cracks deflect and propagate in a different direction, slowing down the overall crack propagation. However, on a flat interface, the crack propagates rapidly in a continuous manner [40–43]. Since the crack propagation is slower and more visible on rough surfaces due to optical contrast, we focus on ice detachment from the abraded surfaces.

The image sequence in Fig. 2B is representative of an ice detachment process, with top-view perspective through the transparent ice layer, with standard video recording at 60 fps (see movie S1). As can be seen by the whitish color of the pillars and following the green line and arrows, ice detachment begins near the force application point and propagates to the other side of the ice block (for simplicity, referred to as front-to-back propagation). The detachment occurs in two stages: first, the ice detaches from the rigid pillars (0–3.9 s), then from the soft areas. This finding may appear surprising, since ice adhesion should be higher on the rigid areas, as they also have higher surface energy (lower contact angle values) and it is known that low elastic modulus and low surface energy facilitates ice detachment [13,44]. However, it can be explained considering the strain, as on a rigid material the ice detachment occurs at lower strains than on a soft material. More strikingly, the direction of crack propagation follows an unexpected opposite propagation at different length scales. When the ice starts to detach, an intuitive front-to-back propagation takes place: first, the ice detaches from the front pillars, then a domino effect causes the ice to detach from the back pillars (t ~ 5 s, v ~ 2.4 mm/s). Only after crack propagation reaches the last pillars on the back side, there is an abrupt adhesion force drop (Figure S4), and afterwards, the ice separates from the soft part until total detachment. However, ice detachment observations highlight that on the individual rigid pillar an opposite, counterintuitive back-to-front propagation occurs, as shown in Fig. 2C and movie S2 (and movie S3 for the non-abraded case). The crack propagation on the individual pillar is initiated on the discontinuity at the back edge of the pillar and then propagates (t ~ 0.5 s, v ~ 2 mm/s) over the pillar to the front side (as highlighted by the zoomed-in insert of magnified pillar in Fig. 2C). The reason why the crack propagates in the opposite direction is described and discussed below, as it becomes clear when mapping the stress distribution on the pillar by numerical simulations.

From experimental results, we hypothesize that stress accumulation leads to the initial ice detachment from the rigid pillar. In particular, the back-to-front propagation on the individual pillars may be due to higher stress building up on the pillar back edge. To confirm this hypothesis, numerical FEM (Finite Element Method) analysis is used to investigate the interfacial stress distribution and to understand whether this reduction in ice adhesion is due to the increase of DL and larger availability of crack initiation sites [23,24,28], or due to higher stress levels on smaller pillars.

The ice-substrate interface shear stresses are depicted in Fig. 3A for the representative case of f_r = 25 % and L = 950 μm (DL = 10.5 cm/cm^2), in brief, “25 %-950 μm”. For comparison, the detailed interface shear stress map for the cases “25 %-950 μm”, “11 %-950 μm” and “25 %-2000 μm” are presented in Figure S5 and Figure S6. In all the considered cases, the applied force F was kept constant. In general, the highest stress concentrations can be found on the front and the back edges of the rigid pillars. Interestingly, the detailed stress map reveals that on the front pillars, i.e., on pillars located close to the force application point, the stress peak is slightly higher on the back edge. This stress distribution is thus compatible with the experimental observation of back-to-front crack propagation on individual pillars (see Fig. 2C), and helps to explain why the crack counterintuitively propagates opposite to the force application direction.

The other two numerically investigated cases, 11 %-950 μm and 25 %-2000 μm, help to assess the effect of the rigid fraction, f_r, and of the pillar width, L. For direct comparison, the non-dimensional stress values τ/τ_{max} on the first row of pillars are computed and summarized in Fig. 3B; τ_{max} is the maximum stress among the three considered cases. The comparison allows us to draw the following conclusions. First, in all three cases, the highest stress concentration on the front pillars is on the back edge, confirming the above discussed trend. Second, the rigid fraction plays a major role in the stress concentration magnitude: the comparison between 25 %-950 μm and 25 %-2000 μm samples reveals similar stresses on the pillar edges, while for the 11 %-950 μm case, significantly higher stresses are observed, which may explain the experimentally observed lower adhesion on this sample. Nonetheless, an analysis based solely on the ice-substrate interface stress distribution does not completely justify the experimental differences observed in ice adhesion. As an example, numerical results show similar stresses for the 25 %-950 μm case compared to 25 %-2000 μm, although experimentally the sample 25 %-950 μm has lower adhesion. As such, considering that our deterministic numerical simulations do not account for the availability of potential crack initiation sites offered by samples with larger discontinuity line, we speculate that the DL length may also play a role. This is supported by the linear relation found between the ice adhesion and the logarithm of the DL length. This relation was detected by representing Fig. 1E using logarithmic scale for the axis of abscissa, see Figure S8.

The results show that one of the discontinuity-enhanced surfaces has an ice adhesion value as low as the soft material. In addition, the decrease of the ice adhesion value when increasing the DL density does not reach saturation for f_r = 11%, see Figure S8. This suggest the possibility to obtain an ice adhesion value below this limit. Based on the explanation of the detachment mechanism, there are three parameter modifications that could be examined in the future to further reduce ice adhesion. First, reducing the rigid fraction (f_r) by increasing the distance between pillars, this approach would lead to an increase of the stress concentrated on the pillar edges, as highlighted by numerical results (see Fig. 3B). Second, increasing the DL length, i.e. reducing the pillars size, while preserving the rigid fraction; based on our results, this should induce more crack initiation sites. Third, increasing the elastic modulus of the rigid areas. A larger mismatch between materials deformability may increase the stress concentration. Potentially, these three modifications could further reduce ice adhesion, but experimental confirmation will be required in future studies.

4. Conclusions

A 3D-printed rigid-soft composite surface showing reduced ice adhesion due to a unique ice detachment mechanism has been developed. This detachment process is based on stress concentration over the elasticity discontinuity line between materials. The unique detachment

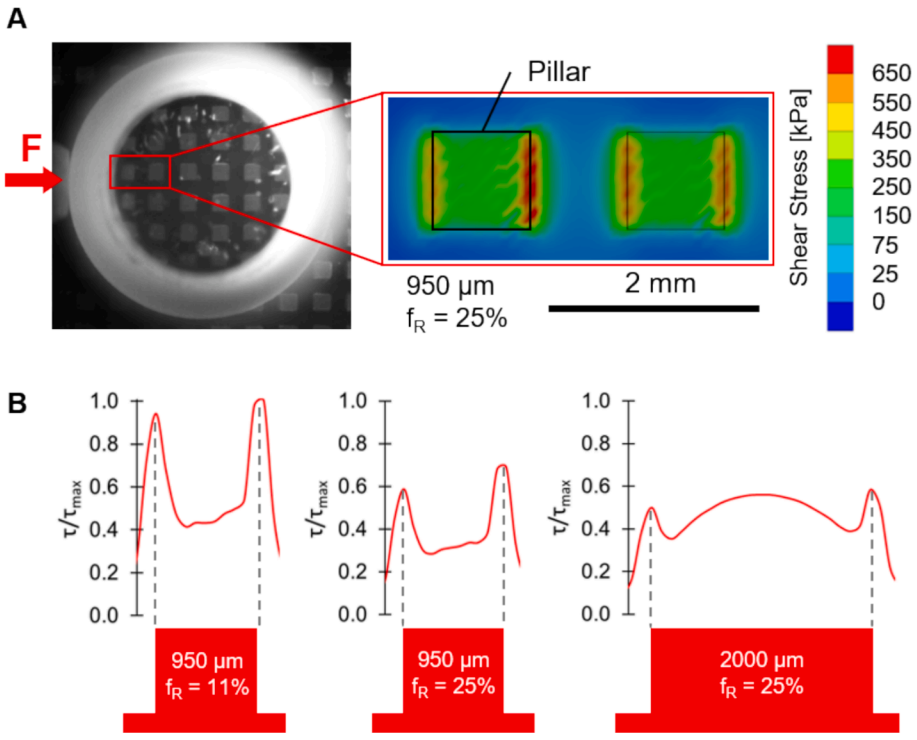

Fig. 3. Stress distribution and crack propagation direction on discontinuity-enhanced icephobic surfaces. A) Shear stress distribution at the ice-substrate interface, as obtained by numerical simulations (sample: 25 %-950 µm). High stress concentrations are located close to the pillar edges, at the transition between rigid and soft areas. Specifically, the highest stress occurs at the back side of the pillar in the front row. This stress distribution explains why at the macroscale the crack propagates front-to-back among pillars, but on the individual pillar the propagation is back-to-front. B) Stress level comparison for the three pillar geometries, taken from their respective first row of pillars. The values are shown as non-dimensional values τ/τ_{max} (τ_{max} is the maximum stress among the three considered cases). All cases show peaks forming on the pillar edges, where discontinuities are located, with the highest peak located on the back edge. The stress concentration becomes more evident for smaller pillars and low rigid fractions, f_R, consistent with the macroscopic observations of ice adhesion in Fig. 1.

process is recorded using a high-speed camera, showing the crack initiation at the discontinuity lines and its propagation first in one direction over the rigid zones and then in the opposite direction over the soft areas. The explanation for this bidirectional crack propagation is unraveled with the support of numerical simulations, which provide the stress distribution at the ice-substrate interface.

Ice detachment mechanism based on stress accumulation has been previously presented in the literature [14,18,23–28]. However, in most cases its justification is based on previous bibliography results instead of direct observation or own analysis. Our study combines for the first time direct observation that cracks initiate at the rigid-soft discontinuity line and propagate first on the rigid part, together with numerical simulations that prove the stress accumulation on the pillar back side. Moreover, lower ice adhesion is reached with increasing the discontinuity line, due to the increase of the potential crack initiation sites, as previously suggested in literature [23–25]. This finding aligns with results from a recently published study proposing a material with sub-surface structure, where the cracks are also observed to start over the rigid parts. Nevertheless, in that study, the size of the rigid areas is smaller, and the ice is not in direct contact with them, as a thin elastic top layer is required [45], making the surface more sensitive to abrasion. From this recompilation of bibliography [14,18,23–28,45] and our results, we observe a tendency where if both materials can be considered as deformable, cracks are more likely to appear in the softer material. Opposite, when one of the materials can be considered as rigid, as on our surfaces, cracks may generate on the harder material.

In addition, another study [33] showed that the combination of materials with different stiffness could reduce (compared to the stiffer material) the adhesion value proportionally to the percentage of softer area without compromising the durability. In that case the minimum dimension of the hard areas was 2 mm. In contrast, our surfaces show an ice adhesion reduction beyond the materials weighted average. Indeed, for the “11 %-200 µm” surface, the adhesion force was equivalent to pure soft material. This would imply an advantage as the material resistance is increased without increasing the ice adhesion value. In addition, our study shows that the critical size (width) of the rigid areas to present the observed detachment mechanism is below 2 mm.

Moreover, it is shown that the surfaces are resistant to mechanical abrasion. In addition, the surfaces are potentially resistant to ambient exposure since PDMS has shown good durability under UV exposure [46]. For practical applications, it is crucial to find a compromise between high mechanical durability and discontinuity line density. In this sense, future work could explore the use of different materials, particularly for the rigid areas, trying to improve their hardness, potentially increasing durability and stress concentration, or their hydrophobicity, which may help to further reduce ice adhesion. In addition, other shapes for the rigid areas and different distributions for the discontinuity line (i.e., other pattern geometries, such as grooves) should be investigated to further improve the performance of discontinuity-enhanced icephobic surfaces. Another line of future research could be to validate the surfaces using types of ice, different to the one tested here (bulk ice). It is known [47] that ice adhesion values can depend on the type of ice (bulk ice, precipitation ice) due to the variation of their mechanical properties. This could affect the detachment mechanism on the discontinuity-enhanced surfaces, as the elastic modulus ratio between the materials composing the interface is a key factor for stress concentration, including ice elastic modulus. As such, the ratio between rigid and soft parts could be considered a design parameter that needs to be adjusted to be effective against different ice densities, which may have different elastic modulus.

CRediT authorship contribution statement

Pablo F. Ibáñez Ibáñez: Writing – original draft, Methodology, Investigation, Funding acquisition, Formal analysis, Data curation, Conceptualization. **Luca Stendardo:** Writing – original draft, Investigation, Formal analysis, Data curation. **Catalina Ospina:** Writing – review & editing, Investigation. **Rajat Chaudhary:** Writing – review & editing, Methodology. **Irene Tagliaro:** Writing – review & editing, Project administration. **Carlo Antonini:** Writing – original draft, Supervision, Project administration, Funding acquisition, Conceptualization.

Declaration of competing interest

The authors declare the following financial interests/personal relationships which may be considered as potential competing interests: Carlo Antonini, Pablo F Ibanez Ibanez, Luca Stendardo, Catalina Ospina, Rajat Chaudhary has patent #Substrato di protezione dal ghiaccio, struttura (102023000026991) pending to University of Milano-Bicocca & University of Granada. If there are other authors, they declare that they have no known competing financial interests or personal relationships that could have appeared to influence the work reported in this paper.

Data availability

Data will be made available on request.

Acknowledgements

This project has received funding from the European Union's Horizon 2020 research and innovation program under the Marie Skłodowska-Curie grant agreement No 956703 (SURFICE Smart surface design for efficient ice protection and control).

P.F.I.I. acknowledges the funding from the Margarita Salas grant (Ministerio de Universidades, Next Generation EU).

The authors are thankful to Anna Maria Coclite (TU Graz, Austria), David Seveno (KU Leuven, Belgium), Valerie Budinger (ISAE Supaero, France) and Daniele Foresti (AcousticaBio, Cambridge, US) for discussing results and commenting the manuscript. Funding for open access charge: Universidad de Granada/CBUA

Appendix A. Supplementary data

Supplementary data to this article can be found online at https://doi.org/10.1016/j.jcis.2024.09.205.

References

[1] Y. Zhuo, S. Xiao, A. Amirfazli, J. He, Z. Zhang, Polysiloxane as icephobic materials – The past, present and the future, Chem. Eng. J. 405 (2021) 127088, https://doi.org/10.1016/j.cej.2020.127088.

[2] A. Dhyani, J. Wang, A.K. Halvey, B. Macdonald, G. Mehta, A. Tuteja, Design and applications of surfaces that control the accretion of matter, Science 373 (2021) eaba5010, https://doi.org/10.1126/science.aba5010.

[3] X. Tian, T. Verho, R.H.A. Ras, Moving superhydrophobic surfaces toward real-world applications, Science 352 (2016) (1979) 142–143, https://doi.org/10.1126/science.aaf2073.

[4] H. Zhang, G. Zhao, S. Wu, Y. Alsaid, W. Zhao, X. Yan, L. Liu, G. Zou, J. Lv, X. He, Z. He, J. Wang, Solar anti-icing surface with enhanced condensate self-removing at extreme environmental conditions, Proc Natl Acad Sci U S A 118 (2021), https://doi.org/10.1073/pnas.2100978118 e2100978118.

[5] I. Tagliaro, A. Cerpelloni, V. Nikiforidis, R. Pillai, C. Antonini, On the development of icephobic surfaces: bridging experiments and simulations, in: The Surface Wettability Effect on Phase Change, Springer International Publishing, 2022, pp. 235–272, https://doi.org/10.1007/978-3-030-82992-6_8.

[6] S. Tian, R. Li, X. Liu, J. Wang, J. Yu, S. Xu, Y. Tian, J. Yang, L. Zhang, Inhibition of Defect-Induced Ice Nucleation, Propagation, and Adhesion by Bioinspired Self-Healing Anti-Icing Coatings, Research 6 (2023) 0140, https://doi.org/10.34133/research.0140.

[7] F.J. Montes Ruiz-Cabello, S. Bermúdez-Romero, P.F. Ibáñez-Ibáñez, M. A. Cabrerizo-Vílchez, M.A. Rodríguez-Valverde, Freezing delay of sessile drops: Probing the impact of contact angle, surface roughness and thermal conductivity, Appl Surf Sci 537 (2021) 147964, https://doi.org/10.1016/j.apsusc.2020.147964.

[8] X. Hao, Z. Sun, S. Wu, T.W. Wang, Y. Liu, Y. Wu, X. He, Q. Liu, F. Zhou, Self-Lubricative Organic-Inorganic Hybrid Coating with Anti-Icing and Anti-Waxing Performances by Grafting Liquid-Like Polydimethylsiloxane, Adv. Mater. Interfaces 9 (2022) 2200160, https://doi.org/10.1002/admi.202200160.

[9] R. Chatterjee, D. Beysens, S. Anand, Delaying Ice and Frost Formation Using Phase-Switching Liquids, Adv. Mater. 31 (2019) 1807812, https://doi.org/10.1002/adma.201807812.

[10] R. Chatterjee, H. Bararnia, S. Anand, A Family of Frost-Resistant and Icephobic Coatings, Adv. Mater. 34 (2022) 2109930, https://doi.org/10.1002/adma.202109930.

[11] P. Guo, Y. Zheng, M. Wen, C. Song, Y. Lin, L. Jiang, Icephobic/Anti-Icing Properties of Micro/Nanostructured Surfaces, Adv. Mater. 24 (2012) 2642–2648, https://doi.org/10.1002/adma.201104412.

[12] N.N. Nguyen, S. Davani, R. Asmatulu, M. Kappl, R. Berger, H.J. Butt, Nano-Capillary Bridges Control the Adhesion of Ice: Implications for Anti-Icing via Superhydrophobic Coatings, ACS Appl Nano Mater 5 (2022) 19017–19024, https://doi.org/10.1021/acsanm.2c04879.

[13] K. Golovin, S.P.R. Kobaku, D.H. Lee, E.T. DiLoreto, J.M. Mabry, A. Tuteja, Designing durable icephobic surfaces, Sci. Adv. 2 (2016) e1501496, https://doi.org/10.1021/acsanm.2c04879.

[14] D.L. Beemer, W. Wang, A.K. Kota, Durable gels with ultra-low adhesion to ice, J Mater Chem A Mater 4 (2016) 18253–18258, https://doi.org/10.1039/C6TA07262C.

[15] V. Vercillo, S. Tonnicchia, J.M. Romano, A. García-Girón, A.I. Aguilar-Morales, S. Alamri, S.S. Dimov, T. Kunze, A.F. Lasagni, E. Bonaccurso, Design Rules for Laser-Treated Icephobic Metallic Surfaces for Aeronautic Applications, Adv. Funct. Mater. 30 (2020) 1910268, https://doi.org/10.1002/ADFM.201910268.

[16] N. Caporale, M. Leemans, L. Birgersson, P.L. Germain, C. Cheroni, G. Borbély, E. Engdahl, C. Lindh, R.B. Bressan, F. Cavallo, N.E. Chorev, G.A. D'Agostino, S. M. Pollard, M.T. Rigoli, E. Tenderini, A.L. Tobon, S. Trattaro, F. Troglio, M. Zanella, Å. Bergman, P. Damdimopoulou, M. Jönsson, W. Kiess, E. Kitraki, H. Kiviranta, E. Nånberg, M. Öberg, P. Rantakokko, C. Rudén, O. Söder, C. G. Bornehag, B. Demeneix, J.B. Fini, C. Gennings, J. Rüegg, J. Sturve, G. Testa, From cohorts to molecules: Adverse impacts of endocrine disrupting mixtures, Science 375 (2022) eabe8244, https://doi.org/10.1126/science.abe8244.

[17] I. Tagliaro, V. Radice, R. Nisticò, C. Antonini, Chitosan electrolyte hydrogel with low ice adhesion properties, Colloids Surf A Physicochem Eng Asp 700 (2024) 134695, https://doi.org/10.1016/J.COLSURFA.2024.134695.

[18] C. Wang, T. Fuller, W. Zhang, K.J. Wynne, Thickness dependence of ice removal stress for a polydimethylsiloxane nanocomposite: Sylgard 184, Langmuir 30 (2014) 12819–12826, https://doi.org/10.1021/la5030444.

[19] K. Golovin, A. Dhyani, M.D. Thouless, A. Tuteja, Low-interfacial toughness materials for effective large-scale deicing, Science 364 (2019) (1979) 371–375, https://doi.org/10.1126/science.aav1266.

[20] T. Chen, X. Dong, L. Han, Q. Cong, Y. Qi, J. Jin, C. Liu, M. Wang, Changing the freezing interface characteristics to reduce the ice adhesion strength, Appl. Therm. Eng. 230 (2023) 120796, https://doi.org/10.1016/j.applthermaleng.2023.120796.

[21] L. Stendardo, A. Milionis, G. Kokkoris, C. Stamatopoulos, C.S. Sharma, R. Kumar, M. Donati, D. Poulikakos, Out-of-Plane Biphilic Surface Structuring for Enhanced Capillary-Driven Dropwise Condensation, Langmuir 39 (2023) 1585–1592, https://doi.org/10.1021/acs.langmuir.2c03029.

[22] W. Deng, S. Ahmad, H. Liu, J. Chen, J. Zhao, Improving boiling heat transfer with hydrophilic/hydrophobic patterned flat surface: A molecular dynamics study, Int. J. Heat Mass Transf. 182 (2022) 121974, https://doi.org/10.1016/j.ijheatmasstransfer.2021.121974.

[23] Z. He, S. Xiao, H. Gao, J. He, Z. Zhang, Multiscale crack initiator promoted super-low ice adhesion surfaces, Soft Matter 13 (2017) 6562–6568, https://doi.org/10.1039/C7SM01511A.

[24] Z. He, Y. Zhuo, J. He, Z. Zhang, Design and preparation of sandwich-like polydimethylsiloxane (PDMS) sponges with super-low ice adhesion, Soft Matter 14 (2018) 4846–4851, https://doi.org/10.1039/C8SM00820E.

[25] Z. He, Y. Zhuo, F. Wang, J. He, Z. Zhang, Understanding the role of hollow sub-surface structures in reducing ice adhesion strength, Soft Matter 15 (2019) 2905–2910, https://doi.org/10.1039/C9SM00024K.

[26] P. Irajizad, A. Al-Bayati, B. Eslami, T. Shafquat, M. Nazari, P. Jafari, V. Kashyap, A. Masoudi, D. Araya, H. Ghasemi, Stress-localized durable icephobic surfaces, Mater. Horiz. 6 (2019) 758–766, https://doi.org/10.1039/C8MH01291A.

[27] J. Wang, M. Wu, J. Liu, F. Xu, T. Hussain, C. Scotchford, X. Hou, Metallic skeleton promoted two-phase durable icephobic layers, J. Colloid Interface Sci. 587 (2021) 47–55, https://doi.org/10.1016/j.jcis.2020.12.027.

[28] X. Jiang, Y. Lin, X. Xuan, Y. Zhuo, J. Wu, J. He, X. Du, Z. Zhang, T. Li, Stiffening surface lowers ice adhesion strength by stress concentration sites, Colloids Surf A Physicochem Eng Asp 666 (2023) 131334, https://doi.org/10.1016/j.colsurfa.2023.131334.

[29] Z. He, Y. Zhuo, F. Wang, J. He, Z. Zhang, Design and preparation of icephobic PDMS-based coatings by introducing an aqueous lubricating layer and macro-crack initiators at the ice-substrate interface, Prog. Org. Coat. 147 (2020) 105737, https://doi.org/10.1016/j.porgcoat.2020.105737.

[30] C. Zeng, Y. Shen, J. Tao, H. Chen, Z. Wang, S. Liu, D. Lu, X. Xie, Rationally Regulating the Mechanical Performance of Porous PDMS Coatings for the

Enhanced Icephobicity toward Large-Scale Ice, Langmuir 38 (2022) 937–944, https://doi.org/10.1021/acs.langmuir.1c02205.
[31] H. Memon, D.S.A. De Focatiis, K.S. Choi, X. Hou, Durability enhancement of low ice adhesion polymeric coatings, Prog. Org. Coat. 151 (2021) 106033, https://doi.org/10.1016/j.porgcoat.2020.106033.
[32] F. Wang, W. Ding, J. He, Z. Zhang, Phase transition enabled durable anti-icing surfaces and its DIY design, Chemical Engineering Journal 360 (2019) 243–249, https://doi.org/10.1016/j.cej.2018.11.224.
[33] G. Sivakumar, J. Jackson, H. Ceylan, S. Sundararajan, An investigation on ice adhesion and wear of surfaces with differential stiffness, Wear 476 (2021) 203662, https://doi.org/10.1016/j.wear.2021.203662.
[34] A. Nistal, A. Ruiz-González, K.L. Choy, Robust icephobic nanocomposite coatings with superior abrasion resistance, Appl. Mater. Today 27 (2022) 101480, https://doi.org/10.1016/j.apmt.2022.101480.
[35] V. Donadei, H. Koivuluoto, E. Sarlin, H. Niemelä-Anttonen, T. Varis, P. Vuoristo, The effect of mechanical and thermal stresses on the performance of lubricated icephobic coatings during cyclic icing/deicing tests, Prog. Org. Coat. 163 (2022) 106614, https://doi.org/10.1016/j.porgcoat.2021.106614.
[36] L. Stendardo, G. Gastaldo, M. Budinger, V. Pommier-Budinger, I. Tagliaro, P. F. Ibáñez-Ibáñez, C. Antonini, Reframing ice adhesion mechanisms on a solid surface, Appl. Surf. Sci. 641 (2023) 158462, https://doi.org/10.1016/j.apsusc.2023.158462.
[37] L. Stendardo, G. Gastaldo, M. Budinger, I. Tagliaro, V. Pommier-Budinger, C. Antonini, Why the adhesion strength is not enough to assess ice adhesion on surfaces, Appl. Surf. Sci. 672 (2024) 160740, https://doi.org/10.1016/j.apsusc.2024.160740.
[38] W.C. Macklin, The density and structure of ice formed by accretion, Q. J. r. Meteorolog. Soc. 88 (1962) 30–50, https://doi.org/10.1002/qj.49708837504.
[39] P.F. Ibáñez-Ibáñez, F.J. Montes Ruiz-Cabello, M.A. Cabrerizo-Vílchez, M. A. Rodríguez-Valverde, Mechanical Durability of Low Ice Adhesion Polydimethylsiloxane Surfaces, ACS Omega 7 (2022) 20741–20749, https://doi.org/10.1021/acsomega.2C01134.
[40] L. Yu, D. Wu, H. Su, S. Li, R. Liu, S. Geng, Influences of Interface Roughness and Loading Direction on Tensile Behavior of Rock-Concrete Bimaterials Under Brazilian Test Conditions, Rock Mech. Rock Eng. 1 (2023) 1–23, https://doi.org/10.1007/s00603-023-03370-8.
[41] J.D. Reedy, Effect of patterned nanoscale interfacial roughness on interfacial toughness: A finite element analysis, J. Mater. Res. 23 (2008) 3056–3065, https://doi.org/10.1557/jmr.2008.0369.
[42] F. Hirsch, M. Kästner, Microscale simulation of adhesive and cohesive failure in rough interfaces, Eng. Fract. Mech. 178 (2017) 416–432, https://doi.org/10.1016/j.engfracmech.2017.02.026.
[43] F.A. Cordisco, P.D. Zavattieri, L.G. Hector, A.F. Bower, Toughness of a patterned interface between two elastically dissimilar solids, Eng. Fract. Mech. 96 (2012) 192–208, https://doi.org/10.1016/j.engfracmech.2012.07.018.
[44] C. Ospina, P.F. Ibáñez-Ibáñez, I. Tagliaro, L. Stendardo, S. Tosatti, C. Antonini, Low ice adhesion on soft surfaces: Elasticity or lubrication effects? J. Colloid Interface Sci. 677 (2025) 494–503, https://doi.org/10.1016/j.jcis.2024.08.042.
[45] C. Chen, P. Fan, D. Zhu, Z. Tian, H. Zhao, L. Wang, R. Peng, M. Zhong, Crack-Initiated Durable Low-Adhesion Trilayer Icephobic Surfaces with Microcone-Array Anchored Porous Sponges and Polydimethylsiloxane Cover, ACS Appl. Mater. Interfaces 15 (2023) 6025–6034, https://doi.org/10.1021/acsami.2c15483.
[46] P.F. Ibáñez-Ibáñez, F.J. Montes Ruiz-Cabello, M.A. Cabrerizo-Vílchez, M. A. Rodríguez-Valverde, Ice adhesion of PDMS surfaces with balanced elastic and water-repellent properties, J Colloid Interface Sci 608 (2022) 792–799, https://doi.org/10.1016/j.jcis.2021.10.005.
[47] S. Rønneberg, Y. Zhuo, C. Laforte, J. He, Z. Zhang, Interlaboratory Study of Ice Adhesion Using Different Techniques, Coatings 9 (2019) 678, https://doi.org/10.3390/coatings9100678.